CHARACTERISTICS OF BRITTLE FRACTURE UNDER GENERAL COMBINED MODES

Yukio Ueda
Welding Research Institute, Osaka University, Japan.

I. INTRODUCTION

Brittle fracture under combined modes was so far studied by Sih *et al.*[1], Erdogan and Sih[2], Cotterell[3], Pook[4] and Shah[5]. The fracture under the combination of Modes I and II was also investigated by, Liebowitz *et al.*[6], Kfouri and Miller[7] and Eftis and Subramonian [8], using a plate with an inclined crack under bi-axial tensile loads. Furthermore, such problems of combined modes as being under uni-axial load have been investigated by many people.

In this paper, the author will summarize the recent research works of his group[9-13] on the initiation characteristics of brittle fracture under various combinations of Modes I, II and III.

A series of fracture tests for various combined modes is carried out using the perfectly brittle material, PMMA (Polymethylmethacrylate), under all possible combinations of Modes I, II, and III.

A series of bi-axial fracture tests is also conducted under the combination of Modes I and II using mild steel (SM 41) specimens. The specimens fractured in a brittle manner with small scale yielding, large scale yielding or under general yielding, depending upon the test temperature. For theoretical prediction of brittle fracture, other than the existing theories, a generalized COD criterion is also employed, which was newly proposed to the case of a crack under combined stress state with large scale yielding or under general yielding[11, 13].

II. FRACTURE OF PERFECTLY BRITTLE MATERIAL UNDER GENERAL COMBINED MODES

1. Criteria for Initiation of Perfectly Brittle Fracture

(1) Criterion based on the maximum tangential stress, $[\sigma_\theta]_{max}$. The maximum tangential stress criterion indicates that the fracture initiates in the normal direction to that of the maximum tangential stress, $[\sigma_\theta]_{max}$, when $[\sigma_\theta]_{max}$ reaches to the critical value[2, 14]. In this direction, the shear stress, $\tau_{r\theta}$, is zero. Therefore, it may be said that the crack initiates in the direction which is normal to the principal stress on the circle of radius r_c and passes through the origin of the coordinates as illustrated in Fig.1 (a). Under the combination of Modes I, II and III, the one of the principal stresses on the circle of

radius r_c illustrated in Fig.1 (b) is the maximum tangential stress, $[\sigma_\theta]_{max}$, when the line normal to the principal stress passes through the origin of the coordinate.

(2) Criterion based on the minimum strain energy density factor, S_{min}. The minimum strain energy density factor criterion depicts that a crack starts to propagate in the direction of the minimum strain energy density factor, S_{min}, when S_{min} reaches to the critical value. This criterion was proposed by Sih[15], but the physical meaning of this criterion is not clear[9].

(3) Criterion based on the maximum strain energy release rate at the propagation of a small kinked crack, $[G^k(\gamma)]_{max}$. Several papers are [16-21] reported as to the stress intensity factors at the tip of a kinked crack as shown in Fig.1 (c).

When a kinked crack propagates in the kinked direction, the strain energy release rate, $G^k(\gamma)$, may be expressed as,

$$G^k(\gamma) = \frac{1-\nu^2}{E}\{K_I(\gamma)^2 + K_{II}(\gamma)^2 + \frac{1}{1-\nu}K_{III}(\gamma)^2\} \tag{1}$$

where ν and E are Poisson's ratio and Young's modulus, respectively. This criterion states that crack propagation initiates in the direction of the maximum strain energy release rate, $[G^k(\gamma)]_{max}$, when it reaches to the critical value.

(4) Criterion based on the maximum strain energy release rate at the initiation of a small kinked crack, $G(\gamma)$. In II.1.(3), the strain energy release rate, $G^k(\gamma)$, for propagation of a small kinked crack in the kinked direction is employed as a fracture criterion. However, strictly speaking, the strain energy release rate, $G(\gamma)$, for initiation of a small kinked crack from the main crack should be used as a fracture criterion under combined stress state, judging from actual fracture behavior.

In this paper, this strain energy release rate, $G(\gamma)$ is also applied, which was derived by the author with the aid of an approximate analytical method[11, 13]. Assuming that the crack opening displacements

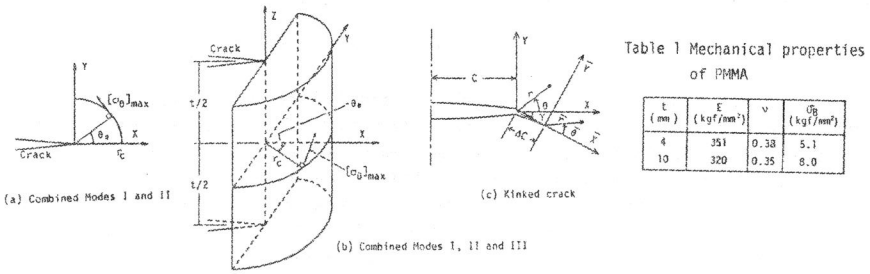

(a) Combined Modes I and II

(b) Combined Modes I, II and III

(c) Kinked crack

Table 1 Mechanical properties of PMMA

t (mm)	E (kgf/mm²)	ν	σ_B (kgf/mm²)
4	351	0.38	5.1
10	320	0.35	8.0

Fig.1 Configuration of cracks

of the infinitesimally small kinked crack can be represented by $K_I(\gamma)$, $K_{II}(\gamma)$ and $K_{III}(\gamma)$ as in the case of a usual straight crack, the strain energy release rate, $G(\gamma)$, can be expressed in the following form:

$$G(\gamma) = \frac{1-\nu^2}{2E}\left(\frac{4}{3+\cos^2\gamma}\right)\left(\frac{1-\gamma/\pi}{1+\gamma/\pi}\right)^{\gamma/2\pi}\cos\frac{\gamma}{2}\{K_I^2(\cos\gamma+\frac{1}{2}+\frac{1}{2}\cos^2\gamma) + 2K_IK_{II}\sin\gamma(1+\cos\gamma)+K_{II}^2(-\frac{3}{2}\cos^2\gamma-\cos\gamma+\frac{9}{2})\} + \frac{1+\nu}{E}\left(\frac{1-\gamma/\pi}{1+\gamma/\pi}\right)^{\gamma/2\pi}\cos\frac{\gamma}{2}K_{III}^2 \tag{2}$$

When the inclination of the kinked crack vanishes, that is $\gamma=0$, Eq.(2) is reduced to the well known form of the strain energy release rate when the straight crack propagates in the same direction as the original one.

2. Fracture Tests

(1) Test specimens. Test specimens for perfectly brittle fracture are made of PMMA. Two different plate thicknesses, 4 mm and 10 mm are used. Their mechanical properties are shown in Table 1. The configuration of specimens for various combined mode tests are illustrated in Figs.2 through 7. The stress intensity factors, K_I, K_{II} and K_{III}, for the notch in each test specimen are summarized in Table 2.

Figure 2 (b) shows a plate specimen with a curvilinear notch for a fracture test under pure Mode II. The angle of the curvilinear crack, ψ, is chosen as 76.9° so that the stress intensity factor of Mode I, K_I, vanishes[19, 22]. Figures 3 (a) and (b) show beam type specimens for fracture tests under pure Mode II and Mode III, respectively. A concentrated vertical load is applied to the midpoint of the specimen which is kept fixed at both ends. The notches are provided at the sections where bending stress vanishes and only shear stresses exist. Although the distribution of shear stress at the section of the beam specimen is parabola in depth, the mean shear stress is used when the stress intensity factors, K_{II} and K_{III}, are calculated.

Figures 4, 6 and 7 show specimens for fracture tests under combined modes Modes I and II, Modes I and III, and Modes I, II and III, respectively. In these specimens, each notch furnished is inclined by angles α and β to the loading direction.

(2) Test procedures. All fracture tests are carried out at room

Table 2 Formulas used to calculate K-value of test specimens

Mode	Test specimen	K - value
I	Fig.6 (a) (α = 90°)	$K_I = \sigma\sqrt{\pi c}\sqrt{\frac{2b}{\pi c}}\left(\tan\frac{\pi c}{2b} + 0.1\sin\frac{\pi c}{b}\right)$ (3) where σ : applied stress, c : length of edge notch, b : half width of specimen
II	Fig.2 (a)	$K_I = \frac{1}{2}\sigma\sqrt{\pi R\sin\psi}\cos\frac{\psi}{2}\frac{-3\cos^2(\psi/2)+10\cos^2(\psi/2)-5}{2-\cos^2(\psi/2)}$, $K_{II} = -\frac{1}{2}\sigma\sqrt{\pi R\sin\psi}\sin\frac{\psi}{2}\frac{-3\cos^2(\psi/2)+8\cos^2(\psi/2)-1}{2-\cos^2(\psi/2)}$ (4) where R : radius of circular arc, ψ : half central angle of sector
	Fig.3 (a)	$K_{II} = \tau\sqrt{\pi c}$ (5) where τ : mean shear stress at beam section
III	Fig.3 (b)	$K_{III} = \tau\sqrt{\pi c}$ (6)
I + II	Fig.4	$K_I = \sigma_y^\infty\sqrt{\pi c}(\sin^2\beta+\lambda\cos^2\beta)\sin^2\alpha$, $K_{II} = \sigma_y^\infty\sqrt{\pi c}(1-\lambda)\sin\beta\cos\beta\sin^2\alpha$ (7)
I + III	Fig.6	$K_{III} = \sigma_y^\infty\sqrt{\pi c}(\sin^2\beta+\lambda\cos^2\beta)\sin\alpha\cos\alpha$ where $\lambda = \sigma_x^\infty/\sigma_y^\infty$, σ_x^∞ and σ_y^∞ : applied stress in the x- and y-direction, respectively, α and β : inclined angle of notch to the plate surface and y-axis, respectively
I + II + III	Fig.7	

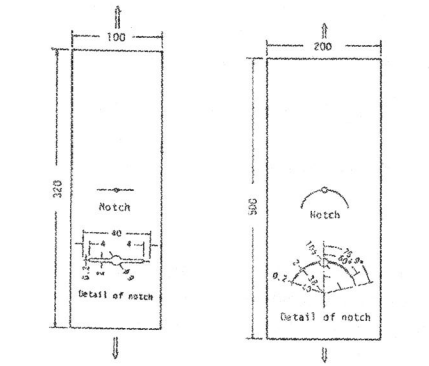

(a) Pure Mode I (Deep notch) (b) Pure Mode II (Curvilinear notch)

Fig.2 Straight side specimens

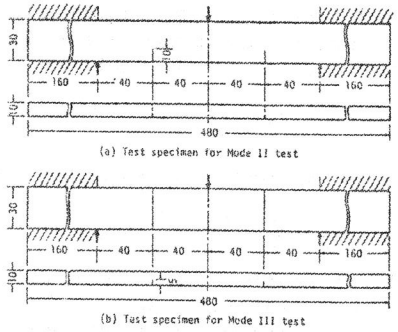

Fig.3 Beam specimen

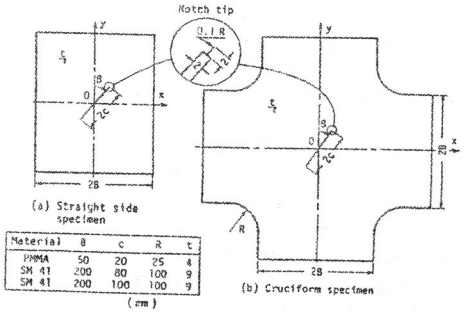

Material	B	C	R	t
PMMA	50	20	25	4
SM 41	200	80	100	9
SM 41	200	100	100	9

(mm)

Fig.4 Specimen for combined Modes I and II

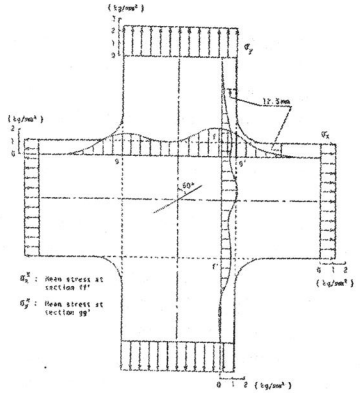

Fig.5 Stress distributions ($\beta = 60°$, $P_x/P_y = 1/2$)

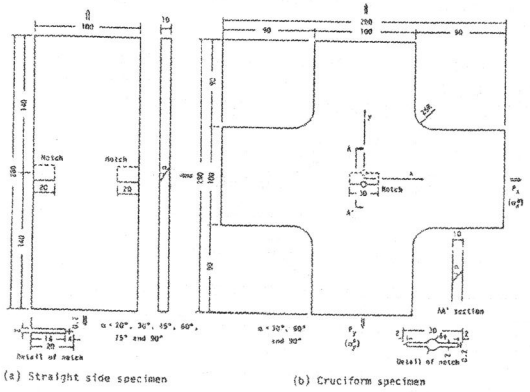

(a) Straight side specimen (b) Cruciform specimen

Fig.6 Specimen for combined Modes I and III

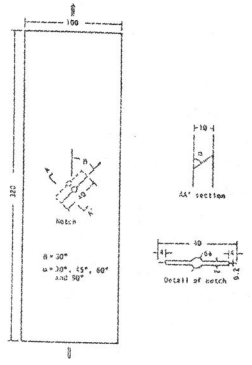

Fig.7 Specimen for combined Modes I, II and III

temperature under the control of displacement at each loading point.

In the bi-axial tensile tests, the load ratios are chosen as 0/1, 1/2 and 1/1 and the loads are applied proportionally in both directions. In this paper, σ_{xe} and σ_{ye} are defined as the mean stresses between points f and f', and g and g', respectively as illustrated in Fig.5. For various combinations of β and P_x/P_y, analyses by the finite element method are also performed, and the relation between these stresses and those along the loading edges, σ_x and σ_y is obtained as,

$$\begin{Bmatrix} \sigma_{xe} \\ \sigma_{ye} \end{Bmatrix} = \begin{bmatrix} 0.80 & -0.09 \\ -0.09 & 0.80 \end{bmatrix} \begin{Bmatrix} \sigma_x \\ \sigma_y \end{Bmatrix} \tag{8}$$

The stress intensity factors of the notch in the cruciform specimen can be evaluated by Eq.(7) in Table 2 substituting σ_{xe} and σ_{ye} into σ_x^∞ and σ_y^∞, respectively.

3. Test Results and Discussions

(1) Brittle fracture under pure Mode I. The fracture toughness value, K_c, of PMMA is 4.6 kgf/mm mm, which was obtained from the tests of the conventional specimens of $\alpha=90°$ which is under pure Mode I in Fig.2 (a).

(2) Brittle fracture under pure Mode II. As for the direction of the initial crack propagation, $-\theta_0$, and the ratio of K_{II} to K_c at fracture, which is denoted by K_{IIf}/K_c, the predicted and the measured ones are represented in Table 3. The fracture angles, $-\theta_0$, predicted by the existing criteria are nearly equal each other and they are close to the measured ones. However, the various criteria predicted different fracture strengths. According to the test results of the beam specimen, the fracture strength agrees well with the predicted one based on $[G(\gamma)]_{max}$ criterion. On the other hand, in the case of the plate specimen with a curvilinear notch, K_{IIf}/K_c=0.91 and is not predicted well by any criterion except by $[\sigma_\theta]_{max}$.

(3) Brittle fracture under pure Mode III. In this case, $G^k(\gamma)$ and $G(\gamma)$ take the same maximum values when $\gamma=0$. The ratio of K_{III} to K_c at fracture, K_{IIIf}/K_c, predicted by them is 0.78 and that by $[\sigma_\theta]_{max}$ criterion is 0.78. Meanwhile, the test results for two specimens indicate that the values of K_{IIIf}/K_c are 0.93 and 1.04. Then, it is seen that $[\sigma_\theta]_{max}$ criterion predicts best the results, under the assumption that the shear stress is regarded uniform in a cross section of the beam.

Table 3 Predicted and measured results of pure Mode II test

	Criterion or test specimen		$-\theta(°)$	K_{IIf}/K_c
Theory	Maximum tangential stress, $[\sigma_\theta]_{max}$		71	0.87
	Maximum energy release rate, $[G^k(\gamma)]_{max}$	Bilby *et al.*[14]	75	0.81
		Hussain *et al.*[15]	75	0.63
	Maximum energy release rate, $[G(\gamma)]_{max}$		72	0.75
Experiment	Plate specimen with curvilinear crack		82	0.91
	Beam specimen with edge cracks		68 73	0.74 0.78
	Cylindrical pipe with circum. crack (AISI 4340)[9]		70~75	0.92

$-\theta$: direction of initial crack propagation
K_{IIf}: stress intensity factor of Mode II at fracture
K_c : fracture toughness

The fracture initiated from some part of the notch front which covers about 5 mm from the top and bottom

surfaces of the specimen shown in Fig.3 (b), and propagated through the width of the beam. After this, the deformation in Mode II prevailed at the newly created crack front and the specimen fractured completely.

(4) Brittle fracture under the combination of Modes I and II. The test results of the cruciform and the straight side specimens are plotted in Figs.8 and 9, which show the direction of propagation of the initial crack, $-\theta_0$, and the fracture stresses, respectively. The curves in these figures are those predicted by the three criteria mentioned in II.1.

From the test results in case of $\beta=90°$, it may be said that the normal stresses parallel to the crack direction have no influence on the fracture stresses.

The directions of propagation and the fracture stresses obtained in this study are in good agreement with the theoretically predicted values based on $[\sigma_\theta]_{max}$ criterion when r_c is assumed to be 0.1 mm.

For the case of $r_c=0$, Erdogan and Sih[2] have studied the crack propagation problems under a general two dimensional stress state. Contrary to this, Cotterell[3] has concluded that the term including r_c in the expression for σ_θ has a significant effect on the direction of initial crack propagation. The test results by Williams and Ewing[14] are in good agreement with the predicted ones when r_c is assumed to be

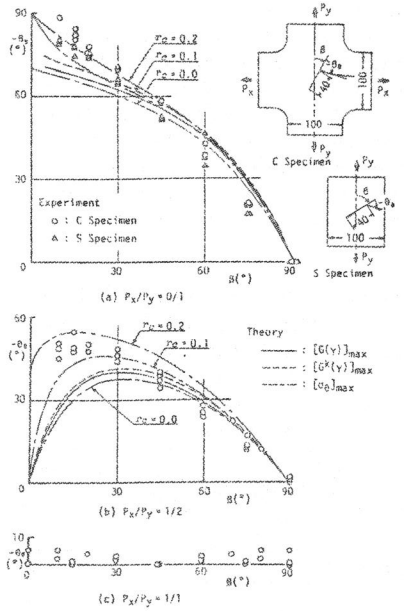

Fig.8 Direction of initial crack propagation under combined Modes I and II (PMMA)

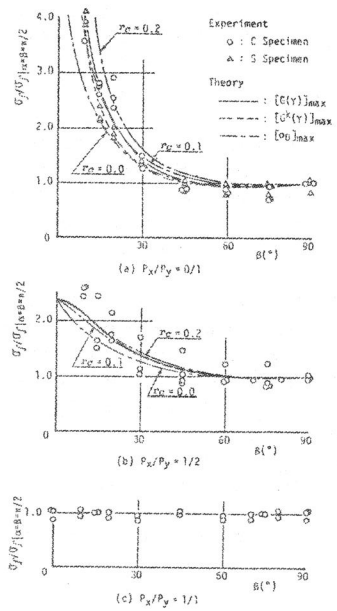

Fig.9 Fracture stresses under combined Modes I and II (PMMA)

0.1 mm. This conclusion is the same as that in this paper. However, the physical meaning and reason why r_c should be 0.1 mm has not been clarified yet.

As observed from Figs.8 and 9, $[G(\gamma)]_{max}$ criterion predicts also fairly accurately the direction of the initial crack propagation and the fracture stress.

The interaction curves of brittle fracture strength under the combination of Modes I and II are derived based on $[\sigma_\theta]_{max}$, $[G^K(\gamma)]_{max}$ and $[G(\gamma)]_{max}$ criteria, and the results are represented in Fig.10 in terms of K_{If}/K_c and K_{IIf}/K_c. Although the test results scatter considerably, with respect to two curves calculated by $[G^K(\gamma)]_{max}$ and $[G(\gamma)]_{max}$ criteria, these two curves may be considered to represent good average curves especially for ○ and ♂.

(5) Brittle fracture under the combination of Modes I and III. The fracture stresses obtained by the tests are plotted in Fig.11, together with the theoretical ones based on $[\sigma_\theta]_{max}$, $[G^K(\gamma)]_{max}$ and $[G(\gamma)]_{max}$ criteria. In this case, the last two criteria take the same maximum values as in the case of pure Mode III fracture when $\gamma=0$. It is also seen in this case that the influence of the normal stress parallel to the notch on the fracture stress can hardly be observed as in the previous case.

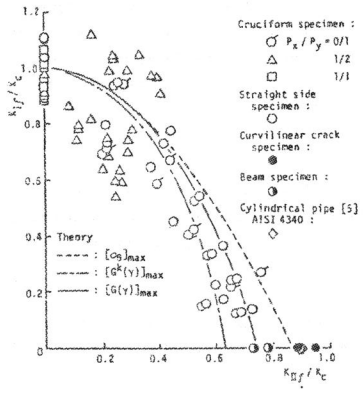

Fig.10 Interaction cruves of K_{If} and K_{IIf}

In the range of small crack angle, α, the measured fracture stresses are somewhat lower than the predicted ones by any criterion. On the other hand, they are in good agreement with the predicted ones based on $[G^K(\gamma)]_{max}$ and $[G(\gamma)]_{max}$ criteria when α is large.

The theoretical interaction curves of the brittle fracture strength under the combination of Modes I and III are calculated and shown in Fig.12 in terms of K_{If}/K_c and K_{IIIf}/K_c. It is observed that the estimated fracture strengths by $[G^K(\gamma)]_{max}$ and $[G(\gamma)]_{max}$ criteria agree with the measured ones except in the range of the small value of K_{III}/K_I which correspond to those for small α.

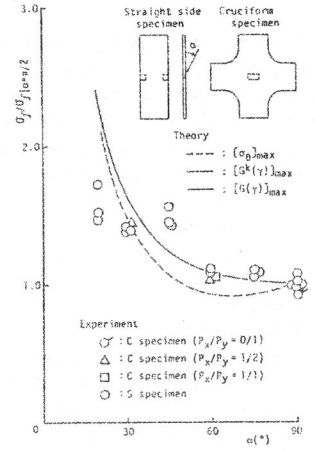

Fig.11 Fracture stresses under combined Modes I and III (PMMA)

There are other experimental studies [5, 4, 23] using AISI 4340, aluminum alloy and HT80. The results are different from those represented in Fig.12. These disagreements may be attributed to the difference of the material whether it is perfectly brittle or semi-brittle and also whether the configuration of specimens and loading conditions are ideal to produce the intended stress distribution.

(6) Brittle fracture under the combination of Modes I, II and III. The experimental fracture stresses are plotted in Fig.13 in comparison with the predicted ones by $[G^k(\gamma)]_{max}$ and $[G(\gamma)]_{max}$ criteria. The fracture stress increases with the decrease of α, and agrees with the predicted ones except in the range of small α.

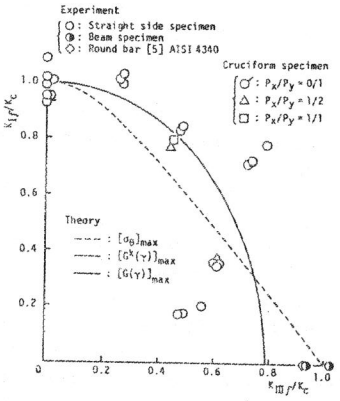

Fig.12 Interaction curves of K_{If} and K_{IIIf}

The interaction curves of brittle fracture under general combined modes are obtained on the above criteria, [12, 13].

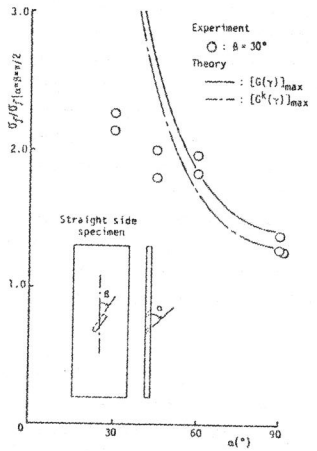

Fig.13 Fracture stresses under combined Modes I, II and III (PMMA)

III. BRITTLE FRACTURE OF ELASTIC-PLASTIC MATERIAL UNDER BI-AXIAL TENSILE LOADS

1. Criteria for Initiation of Brittle Fracture with Yielding

(1) Criterion based on the maximum strain energy release rate at the initiation of small kinked crack. As is known from the discussions made in II,3, that $[G^k(\gamma)]_{max}$ and $[G(\gamma)]_{max}$ criteria are better than the others in predicting the initiation of the perfectly brittle fracture under general combined modes, these criteria are expected to be applicable especially to the brittle fracture even with small scale yielding under bi-axial tensile loads.

(2) Criterion based on crack opening displacement, Φ. COD criterion has been proposed originally as a fracture criterion especially in the field of a fracture with large scale yielding or under general yielding of pure Modes I and III, and the applicability of this criterion has been well appreciated. In parallel with this, the strip yield model has been proposed as an elastic-plastic crack model for calculation of COD by Dugdale[24] and Bilby *et al.*[25]. Further, a strip yield model under combined modes is proposed by Sakai and Sakano[23]. The size of the

plastic zone in the strip yield model does not indicate the actual one but only conceptual, and this becomes a reasonable value only in the limiting case of $\beta=90°$ and $P_x/P_y=0/1$. Essentially, the size and the extending direction of the plastic zone should be closely related to COD. However, it is very difficult to take into account of the respective component of stress in the analytical elastic-plastic crack model proposed so far.

There is no problem if COD is calculated theoretically, such as by the elastic-plastic stress analysis using the finite element method. The criterion based on COD may be generalized and expressed that the crack propagation initiates in the direction perpendicular to the COD vector, Φ, when it reaches to the critical value, Φ_{cr}, [11, 13].

2. Fracture Tests

(1) Test specimens. Test specimens are made of mild steel (SM 41) of which mechanical properties and chemical compositions are shown in Table 4. A series of the deep notch tests is conducted to obtain the fracture toughness of the material, whose result is shown in Fig.14.

Cruciform specimens and straight side ones are prepared as shown in Fig.4. Each one contains a center notch perpendicular to the plate surface but inclined at an angle, β, to the vertical direction, which is machined through thickness.

(2) Test procedures. The bi-axial testing machine installed at Welding Research Institute of Osaka University is used. The machine is composed of a 300 ton vertical testing machine and a specially designed 150 ton horizontal testing machine which can move vertically during the test in accordance with the vertical displacement of the specimen as illustrated in Fig.15.

Table 4 Mechanical properties and chemical compositions of SM 41

Mechanical properties			Chemical compositions (%)				
σ_s (kgf/mm²)	σ_B (kgf/mm²)	EL. (%)	C	Si	Mn	P	S
41	50	26	0.14	0.25	0.86	0.028	0.014

The fracture tests are performed at an approximately constant temperature of -140°C and in the temperature range from -90°C to -60°C. At the former temperature, the cruciform and the straight side specimens are tested of which notch lengths are 160 mm, and the fracture of the specimens occurred in a brittle manner with small scale yielding. Contrary to this, in the latter temperature range, only the

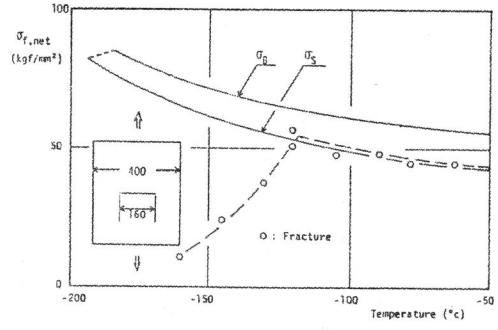

Fig.14 Results of deep notch test

cruciform one is tested, of which notch length is 200 mm and the specimens fractured in brittle manner with large scale yielding or under general yielding.

During the tests, the direction of the initial crack propagation and the fracture stress are measured on all specimens. Additionally, the crack opening displacements are measured on some specimens using clip-gages in the fracture test with large scale yielding or under general yielding. For the measurement of COD, two clip-gages are attached to the specimen between points, A and B, and B and C, as shown in Fig.16. From the displacements between these points, the resultant COD under a combination of Modes I and II can be calculated and decomposed into the two corresponding components to Modes I and II.

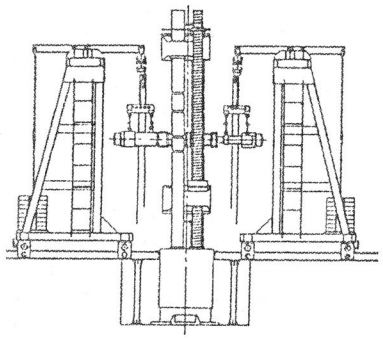

Fig.15 Appearance of bi-axial testing machine

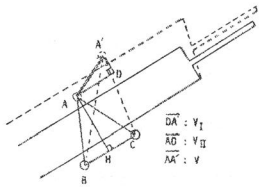

Fig.16 Measurement of COD under combined Modes I and II

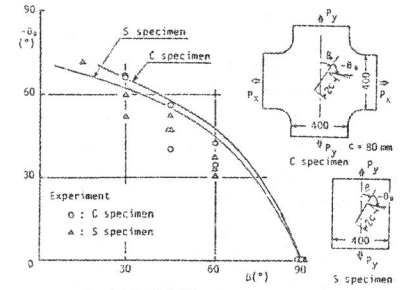

Fig.17 Direction of initial crack propagation under combined Modes I and II (SM 41, small scale yielding)

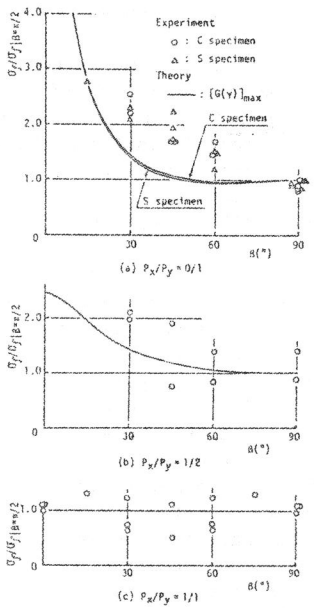

Fig.18 Fracture stresses under combined Modes I and II (SM 41, small scale yielding)

3. Test Results and Discussions

(1) Brittle fracture with small scale yielding. The direction of initial crack propagation and the fracture stresses are plotted against the crack angle, β, in Figs.17 and 18, respectively. The solid lines in these figures represent the theoretical values predicted based on $[G(\gamma)]_{max}$ criterion.

The test results and the predicted ones are in good agreement concerning the direction of the initial crack propagation, but not for the fracture stresses. In the case of the bi-axial load ratio of 1/1, the test results are scattered around the theoretical curve. On the other hand, the test data are higher than the predicted curves when the bi-axial load ratio P_x/P_y is 0/1 and 1/2, and the differences between them are most predominant when the crack angle, β, is 45°.

To investigate these differences, the critical strain energy release rates at fracture, G_f, are plotted against the stress intensity factor of Mode II, K_{II}, in Fig.19 (a), where G_c is the fracture toughness evaluated from the deep notch test. For comparison, the results on PMMA specimens are also shown in the same manner in Fig.19 (b). The former is dependent upon K_{II} and the latter is not. In these figures, the scattering bands of the data are indicated by two solid lines.

In the case of PMMA which is an elastic and perfectly brittle material, the slip does not take place. The energy is stored in the core region surrounding the notch tip due to the Mode II deformation and its release rate is converted completely to the energy release rate at fracture. Consequently, the value of G_f may not show dependency on K_{II} value. On the other hand, in the case of SM 41, which is an elastic-plastic material, the supplied energy is partly dissipated in forming slip lines near the notch tip and the dissipated energy is non-reversible. Such slip line forms at an angle of 45° to the direction of the principal stress. Therefore, the in-plane shear deformation under Mode II produces slip lines most effectively when the crack angle, β, coincides with the direction of slip lines. This may be one of the main reasons why the strain energy release rate at fracture, G_f, increases as the value of Mode II stress intensity factor, K_{II} increases as illustrated in Fig.19 (a).

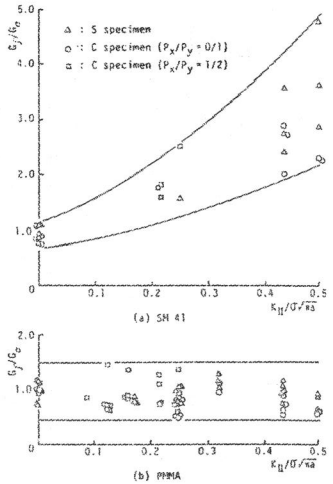

Fig.19 Variation of strain energy release rate at fracture with K_{II}

(2) Brittle fracture with large scale yielding or under general yielding. It is very difficult to measure COD always successfully under combined stress modes

at the test, and it is complicated to convert the measured COD to that at the notch tip. In contrast with this, COD can be obtained much easier by the elastic-plastic stress analyses using the finite element method. In the analyses, the mesh size near the notch tip is kept the same regardless of the notch angle, β and the bi-axial load ratio, P_x/P_y, and the meshes near the notch tip is illustrated in Fig.21. The analyses are performed on the test specimens for all possible combinations of β and P_x/P_y . The strain hardening ratio, H', is assumed as $E/100$, where E is Young's modulus.

In order to confirm the accuracy of the calculated COD, it is compared with the measured COD for several specimens. One example of these is shown in Fig.20. As the load exceeds about 100 tons, the measured COD becomes greater than the calculated one. This may be attributed to the short slow crack growth in the actual test specimen. Taking this into account, the calculated COD is considered to agree well with the measured one. In

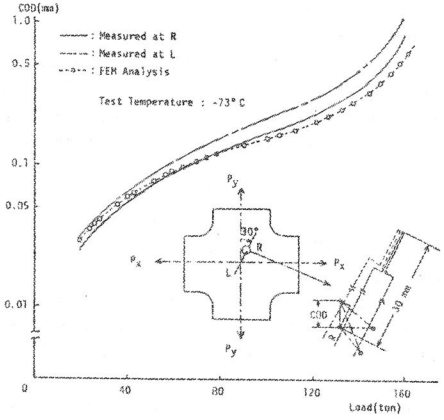

Fig.20 Comparison of measured COD with calculated one

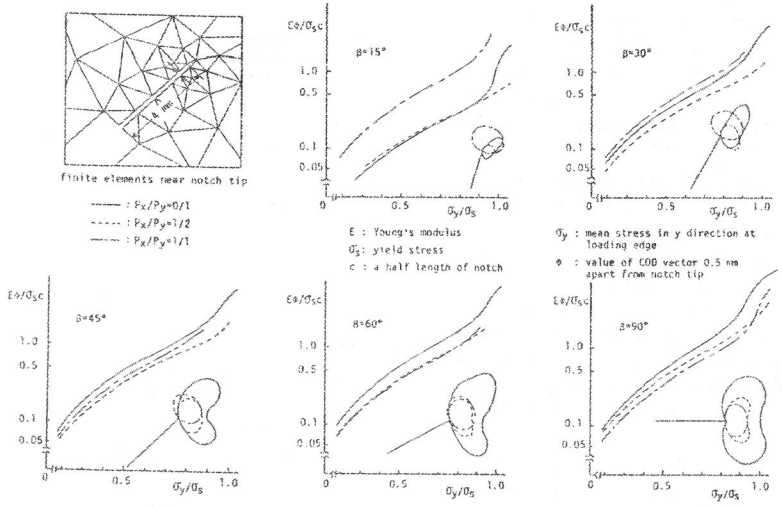

Fig.21 Mean stress-COD curves and spread of plastic zone at $\sigma_y/\sigma_S = 0.75$

the following discussion, the calculated COD at the location of 0.5 mm apart from the notch tip will be used as that at the notch tip.

Figure 21 shows the relation between the calculated mean stress and the COD, and the plastic zone sizes for all combinations of the notch inclination angles and the bi-axial load ratios. The shape and the spread of the plastic zone are influenced by the notch angle and the bi-axial load ratio, P_x/P_y, except when P_x/P_y=1/1.

The testing temperature influences the yield stress as represented in Fig.14. Therefore, the stress analysis for each specimen should be performed using the corresponding value of the yield stress to the testing temperature. However, this requires a plenty of computation time. To reduce this, it was assumed that H'/E is same for the same value of $\bar{\varepsilon}/\varepsilon_S$ at every test temperatures, where $\bar{\varepsilon}$ and ε_S are the equivalent strain and the yield strain, respectively. This assumption leads that the relation between $\Phi E/\sigma_S c$ and σ_y/σ_S is completely the same for any specimen being same in shape[10].

Hereafter, the COD at fracture, Φ_f, is calculated for the fracture stress, σ_y, using the nondimensionalized relations between $\Phi E/\sigma_S c$ and σ_y/σ_S shown in Fig.21, and adopting the yield stress, σ_S , at the corresponding testing temperature.

Figures 22 represents the relations between the notch inclination angle, β, and the direction of initial crack propagation, -θ. The solid lines represent the direction estimated under the assumption that the fracture initiates in the direction perpendicular to the COD vector at the notch tip. In the cases of β=15°, 30° and 45°, except β=60° and 90°, at P_x/P_y=0/1, the fracture initiates in the direction of β+(-θ)=45°, that is, the direction of the maximum shear stress in the plate without a notch. In these cases, the fracture surface is normal to the plate surface and shows a shear appearance. Hereafter, this type of fracture will be called as shear fracture. The remaining specimens fractured in brittle manner. As a particular case of P_x/P_y=1/1, the predicted direction coincides with the axis of the notch as indicated in Fig.22 (c).

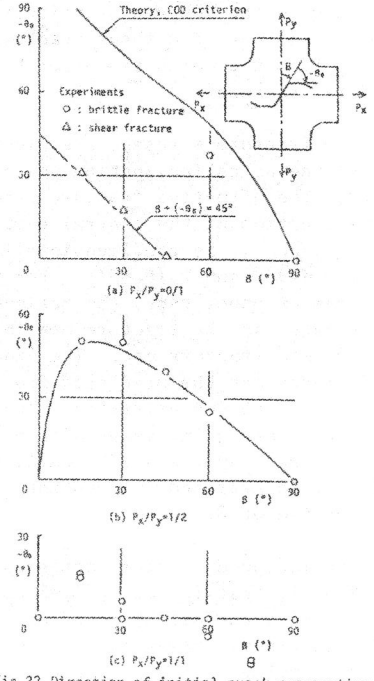

Fig.22 Direction of initial crack propagation under combined Modes I and II (SM 41, large scale yielding)

The predicted directions show good agreement with the measured ones except

when the shear fracture takes place. The main reason of this agreement may be due to the fact that the COD vector at the notch tip is closely related to that of the stretched zone formed prior to the fracture, and that the fracture initiates in the direction perpendicular to the stretched zone[26].

Here, the COD criterion is applied also to the brittle fracture with small scale yielding mentioned in III.3.(1). However, it is recognized that the direction of initial crack propagation predicted by $[G(\gamma)]_{max}$ criterion shows better agreement with the measured one than that by the COD vector criterion. Therefore, it may be said that each criterion should be applied to an appropriate case.

Moreover, when the notch is subjected to such loads as to produce pure Mode II deformation and such temperature as to fracture in a brittle manner of pure Mode I with large scale yielding or under general yielding, the COD vector will be parallel to the notch. In this case, the direction of initial crack propagation may be predicted to be perpendicular to the notch according to the COD vector criterion. However, in fact, the shear crack will proceed from the notch tip prior to the complete fracture.

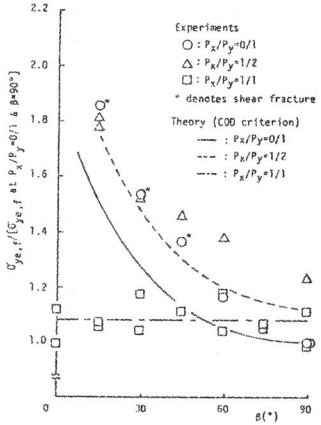

Fig.23 Fracture stresses under combined Modes I and II (SM 41, large scale yielding)

The fracture stresses are plotted against the notch inclination angle, β, in Fig.23. The effective fracture stress in the y-direction at the central part of the specimen, $\sigma_{ye,f}$, is nondimensionalized by that for β=90° and P_x/P_y=0/1. For the fractures of shear type, the maximum stress is indicated as the fracture one instead of the complete fracture one. The lines in Fig.23 represent the predicted fracture stresses by the COD criterion. The fracture stresses increases with a decrease of β when P_x/P_y=0/1 and 1/2, while that for P_x/P_y=1/1 is kept nearly constant irrespective of β.

The measured fracture stresses under pure Mode I, that is for P_x/P_y=1 or β=90° distribute in the neighborhood of the predicted lines. However, those under various combined modes of I and II, except the above ones, scatter above the predicted lines.

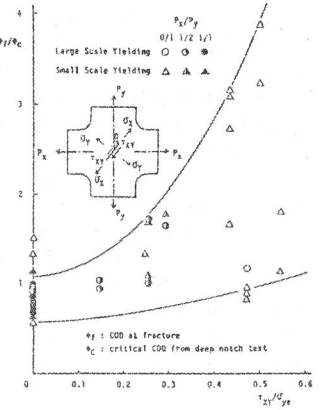

Fig.24 Variation of COD at fracture with shear stress parallel to notch (SM 41)

Using the same test results, the COD at fracture, Φ_f, is plotted against the shear stress, τ_{xy}, in Fig.24, where Φ_c is the critical COD or the fracture toughness evaluated at fracture from the deep notch test. The results obtained from the brittle fracture tests with small scale yielding are also plotted in the same figure. This figure indicates that the COD at fracture, Φ_f, increases with an increase of the shear stress. Therefore, if it is assumed that the COD at fracture, Φ_f, is not affected by the in-plane shear deformation, the COD criterion predicts the conservative fracture strength and may be said practically applicable.

Table 5 Comparison of shear fracture with brittle fracture

Type of fracture	Profile of crack propagation	Spread of plastic zone at fracture
Brittle fracture β = 45° P_x/P_y = 0/1 Test temp. ; -140°C		
Shear fracture β = 45° P_x/P_y = 0/1 Test temp. ; -75°C	Original notch tip 40 80 L (mm)	

As mentioned before, the shear fracture initiates from the notch tip in the case of β=15°, 30° and 45° under uni-axial tension. Here, the shear fracture is characterized by comparing it with the brittle one. As an example, the case of β=45° and P_x/P_y=0/1 is chosen, and a comparison is made between the brittle fracture at -140°C and the shear one at -75°C. Table 5 represents the crack path and the plastic zone. In the shear fracture, the plastic zone at fracture extends nearly all over the test specimen. The horizontally sliding displacement is produced between the upper and the lower surfaces of the notch, and the crack propagates in the same direction as the maximum shear stress of the specimen without a notch. The average shear stress along the prolonged line of the shear crack is nearly equal to a half of the tensile strength. Moreover, while cleavage appearance can be seen at the tip of notch of the specimen fractured in a brittle manner, there can be observed the large stretched zone at the tip of notch and the elongated dimple pattern at the prolonged part of the crack in a shear manner. Since the equiaxised dimple pattern can be seen in the shear fracture, the component of the shear stress parallel to the shear crack is considered to play a predominant role in such fracture behavior.

IV. CONCLUSIONS

The brittle fracture initiation characteristics under arbitrary combination of Modes I, II and III are investigated both theoretically and experimentally. From the results, the following conclusions are drawn.

For the perfectly brittle fracture;

(1) The uniform stress parallel to the notch has little effect on the

direction of initial crack propagation and the fracture strength.
(2) The criterion based on the maximum strain energy release rate, $[G^K(\gamma)]_{max}$ or $[G(\gamma)]_{max}$ is most suitable in predicting the direction of initial crack propagation and the fracture strength under combined modes.

For the brittle fracture with small scale yielding;
(3) The direction of initial crack propagation is well predicted by the $[G(\gamma)]_{max}$ criterion.
(4) The measured fracture strength is higher than the predicted one by the $[G(\gamma)]_{max}$ criterion, and increases with an increase of Mode II deformation. This may be attributed to the loss of the strain energy stored in the core region surrounding the notch tip, which is dissipated to the plastic work due to Mode II deformation.

For the brittle fracture with large scale yielding or under general yielding;
(5) The uniform stress parallel to the notch has influence on the size, the extending direction of the plastic zone, and consequently on COD. Therefore, this stress affects the fracture strength.
(6) The brittle fracture initiates in the direction perpendicular to the COD vector.
(7) The measured fracture strength is higher than the predicted one by the COD criterion, and increases with an increase of Mode II deformation, which is in the similar manner to the brittle fracture with small scale yielding.
(8) From the conclusions described in (4) and (7), the strength of brittle fracture with yielding may be conservatively estimated by the criterion based on $[G(\gamma)]_{max}$ or COD vector when the size of the plastic zone is small or large, respectively.

The author wish to express his gratitude to his colleagues, especially to Dr. M. Aoki, Kobe Steel Ltd., and Prof. T. Yao, Hiroshima National Univ., Japan, for their assistance and advice in writing this manuscript.

REFERENCES

[1] G.C.Sih, P.C.Paris and F.Erdogan, Crack Tip Stress Intensity Factors for Plane Extension and Plate Bending Problems, Trans. ASME, J.Appli.Mech., Vol.29 (1962), 306-312.
[2] F.Erdogan and G.C.Sih, On the Crack Extension in Plates under Plane Loading and Transverse Shear, Trans. ASME, J.Basic Eng., 85D (1963), 519-527.
[3] B.Cotterell, Notes on the Paths and Stability of Cracks, Int.J.Frac.Mech., 2 (1966), 526.
[4] L.P.Pook, The Effect of Crack Angle on Fracture Toughness, Eng.Frac.Mech., Vol.3 (1971), 205-218.
[5] R.C.Shah, Fracture under Combined Modes in 4340 Steel, ASTM STP 560 (1974), 29-52.
[6] H.Liebowitz, J.Eftis and D.L.Jones, Some Recent Theoretical and Experimental Developments in Fracture Mechanics, Advances in Research on the Strength and Fracture of Meterials, Vol.1 (1977), ICF 4, 695-721.
[7] A.P.Kfouri and K.J.Miller, The Effect of Load Bi-axiality on the Fracture Toughness Parameters J and G, Fracture, Waterloo, Canada, Vol.3 (1977), ICF 4,.
[8] J.Eftis and N.Subramonian, The Inclined Crack under Bi-axial Load, Eng.Frac.Mech., Vol.10 (1978), 43-67.
[9] Y.Ueda, K.Ikeda, T.Yao, M.Aoki, T.Yoshie and T.Shirakura, Brittle Fracture Initiation Characteristics under Bi-axial Loading, J.Soc.Naval Arch. of Japan, Vol.139 (1976), 240-247 (in Japanese), and Fracture, Waterloo, Canada, Vol.2 (1977), ICF 4, 173-182.
[10] Y.Ueda, K.Ikeda, T.Yao, M.Aoki, T.Yoshie, T.Shirakura and S.Shibasaki, Brittle Fracture Initiation Characteristics under Bi-axial Loading (2nd Report), J.Soc.Naval Arch. of Japan, Vol.142 (1977), 127-134 (in Japanese), and Trans. JWRI (Japan Welding Research Institute of Osaka University), Vol.8, No.1 (1979), 121-130.
[11] Y.Ueda, K.Ikeda, T.Yao, M.Aoki, S.Shibasaki and T.Shirakura, Brittle Fracture Initiation Characteristics under Bi-axial Tensile Load with Large Scale Yielding and General Yielding, Advances in Fr. Research, Cannes, France, Vol.5 (1981), ICF5, 2321-2328.
[12] Y.Ueda, K.Ikeda, T.Yao, M.Aoki and S.Shibasaki, Characteristics of Brittle Fracture under General Combined Modes, J.Soc.Naval Arch. of Japan, Vol.144 (1978), 412-419 (in Japanese), and Trans. JWRI, Vol.9, No.2 (1980), 95-104.
[13] Y.Ueda, K.Ikeda, T.Yao and M.Aoki, Characteristics of Fracture under General Combined Modes Including Those Under Bi-Axial Tensile Loads, To be published in Eng.Frac.Mech.
[14] J.G.Williams and P.D.Ewing, Fracture under Complex Stress - The Angled Crack Problem, Int.J.Frac.Mech., Vol.8 (1972), No.4 441-446.
[15] G.C.Sih and B.C.K.Cha, A Fracture Criterion for Three Dimensional Crack Problem, Eng.Frac.Mech., 6 (1974), 699-723.
[16] B.A.Bilby and G.E.Cardew, The Crack with Kinked Tip, Int.J.Frac.Mech.,Vol.11, No.4 (1975), 708-712.
[17] A.A.Khrapkov, The First Basic Problem for a Notch at the Apex of an Infinite Wedge, Int.J.Frac.Mech., Vol.7, No.4 (1971), 373-382.
[18] S.N.Chatterjee, The Stress Field in the Neighborhood of a Branched Crack in an Infinite Elastic Sheet, Int.J.Solid and Structures, Vol.11 (1975), 521-538.
[19] M.A.Hussain, S.L.Pu and J.Underwood, Strain Energy Release Rate for a Crack under Combined Mode I and II, ASTM STP 560 (1974), 2-28.
[20] G.C.Sih, Stress Distribution near Internal Crack Tips for Longitudinal Shear Problems, Trans. ASME, J.Appl.Mech., 3 (1975), 51-58.
[21] E.Smith, A Note on Crack-forming in Anti-plane Strain Deformation, Int.J.Frac., Vol.9, No.2 (1973), 181-183.
[22] M.A.Hussain and S.L.Pu, Slip Phenomenon for a Circular Inclusion, Trans. ASME, J.Appl.Mech., Vol.38 (1971), No.3, 627-633.
[23] K.Sakai and K.Sakano, A Study on Brittle Fracture Initiation under Combined Modes, J.Soc.Naval Arch. of Japan, Vol.139 (1976), 257-264

(in Japanese).
[24] D.S.Dugdale, Yielding of Steel Sheets Containing Slits, J.Mech.Physics and Solids, 8 (1960), 100-104.
[25] B.A.Bilby, A.H.Cottrell and K.H.Swinden, The Spread of Plastic Yield from a Notch, Proc.Roy.Soc., A279 (1964), 304-314.
[26] A.Ohtsuka, T.Miyata, S.Nishimura and N.Kasai, The Stretched Zone and COD-criterion on the Fracture, J.Soc.Naval Arch. of Japan, Vol.136 (1974), 249-257 (in Japanese).